nature chemistry

ARTICLES

https://doi.org/10.1038/s41557-019-0325-7

Super-resolution labelling with Action-PAINT

Ninning Liu[1,3], Mingjie Dai[1,2,3*], Sinem K. Saka[1] and Peng Yin[1,2*]

Recent advances in localization-based super-resolution microscopy have enabled researchers to visualize single molecular features down to individual molecular components (~5 nm), but do not yet allow manipulation of single-molecule targets in a user-prescribed, context-dependent manner. Here we report an 'Action-PAINT' (PAINT, point accumulation for imaging in nanoscale topography) strategy for super-resolution labelling upon visualization on single molecules. This approach monitors and localizes DNA binding events in real time with DNA-PAINT, and upon visualization of binding to a desired location, photo-crosslinks the DNA to affix the molecular label. We showed the efficiency of 3-cyanovinylcarbazole nucleoside photo-inducible crosslinking on single molecular targets and developed a software package for real-time super-resolution imaging and crosslinking control. We then benchmarked our super-resolution labelling method on synthetic DNA nanostructures and demonstrated targeted multipoint labelling on various complex patterns with 30 nm selectivity. Finally, we performed targeted in situ labelling on fixed microtubule samples with a 40 nm target size and custom-controlled, subdiffraction spacing.

The ability to observe and in situ modify biological systems on the molecular scale is critical to study biology in health and in disease. Super-resolution imaging enables researchers to 'see the previously invisible' by breaking the diffraction limit of light and precisely visualizing biology on the molecular scale, and has broadly transformed biomedical research[1–3]. However, a comparable optical capability for labelling and perturbing biological systems with nanometre precision is lacking.

Although photolithography and optical masking methods have proved to be successful in the high-resolution manufacturing of solid-state materials (for example, semiconductors)[4], they are less suitable for manipulating biological samples because the positions of the targets of interest are not known a priori. Optical controls in biology, such as optogenetics[5], typically have a spatial resolution limited by the diffraction limit of light, whereas contact-based controls, such as atomic force microscopes[6], are often disruptive and lack the depth of sample penetration.

An optical approach that could both 'visualize' biological structures at the molecular scale, and upon visualization, react to the detected features to 'label' the underlying biological system with a molecular cargo or uniquely addressable physical handle (for example, a DNA barcode) at an equal nanometric precision is desired (Fig. 1a). Such a capability of 'labelling upon visualization' will not only allow researchers to 'see the previously invisible', but also enable them to 'touch the previously inaccessible', which presents a possible platform for the precise, single-component-level interrogation of biomolecular systems, which includes the perturbation and delivery of a functional cargo to specific protein targets, site-specific labelling and the purification of macromolecular complexes, and more (See discussion).

Recent advances in localization-based super-resolution microscopy methods (for example, stochastic optical reconstruction microscopy (STORM)[7,8], photoactivation localization microscopy (PALM)[9,10] and point accumulation for imaging in nanoscale topography (PAINT)[11,12]) have allowed researchers to optically visualize molecular features well below the diffraction limit and down to individual molecular components (~5 nm) (refs [13–21]), but do not yet allow observation followed by manipulation or labelling of single-molecule targets in a sequential manner, which is particularly important for studying complex, spatially varying and context-dependent biological systems. We termed this capability super-resolution labelling upon visualization. Super-resolution microscopy methods based on the PAINT principle[11,12,22–24] provide a natural path towards such a capability. In these methods, a population of fluorophore-conjugated affinity probes transiently and repetitively bind to each of the imaging targets to produce apparent blinkings that can then be individually localized with a high precision to synthesize the final super-resolution image. In contrast to other localization microscopy techniques, PAINT-based methods provide the extra benefit that, at any moment, typically only one affinity probe is bound to the imaging sample within a diffraction-limited area. This makes a light-induced targeting approach possible—if an activating light pulse can be introduced precisely at this moment (that is, during the transient association between the affinity probe and a desired target), this spatiotemporal co-localization would allow selective molecular manipulation (the 'action') to be performed on the target (Fig. 1b). We termed this approach 'Action-PAINT'[25].

In this work, we designed and implemented such a strategy for super-resolution labelling on single molecules based on our previous conceptual proposal[25]. The design combines our previously developed DNA-PAINT super-resolution microscopy method, and a fast, photoinducible crosslinking chemistry[26,27]. We first assayed the efficiency of 3-cyanovinylcarbazole nucleoside (CNVK) photoinducible crosslinking on single molecular targets, and developed a software package for real-time super-resolution image analysis and crosslinking control. Then, we benchmarked our super-resolution labelling method on synthetic DNA nanostructures and demonstrated a high efficiency-per-target (up to 65%) labelling, and targeted single-molecule labelling with a 70 nm selectivity (33% overall success rate). We showed that our method is capable of performing multipoint labelling on various complex 6-choose-3 patterns with a 30 nm selectivity (69% success rate for at least 2 on-target labelling, 12% overall success rate, 18× higher than random labelling). Finally, we showed that our method is also compatible with in situ super-resolution imaging, and demonstrated a successful targeted labelling on fixed microtubule samples with a 40 nm label size and variable, diffraction-unlimited spacings (78% on-target labelling, 24% off-target labelling, normalized 4.2× on-/off-target labelling

[1]Wyss Institute for Biologically Inspired Engineering, Harvard University, Boston, MA, USA. [2]Department of Systems Biology, Harvard Medical School, Boston, MA, USA. [3]These authors contributed equally: Ninning Liu, Mingjie Dai. *e-mail: mingjie_dai@hms.harvard.edu; py@hms.harvard.edu

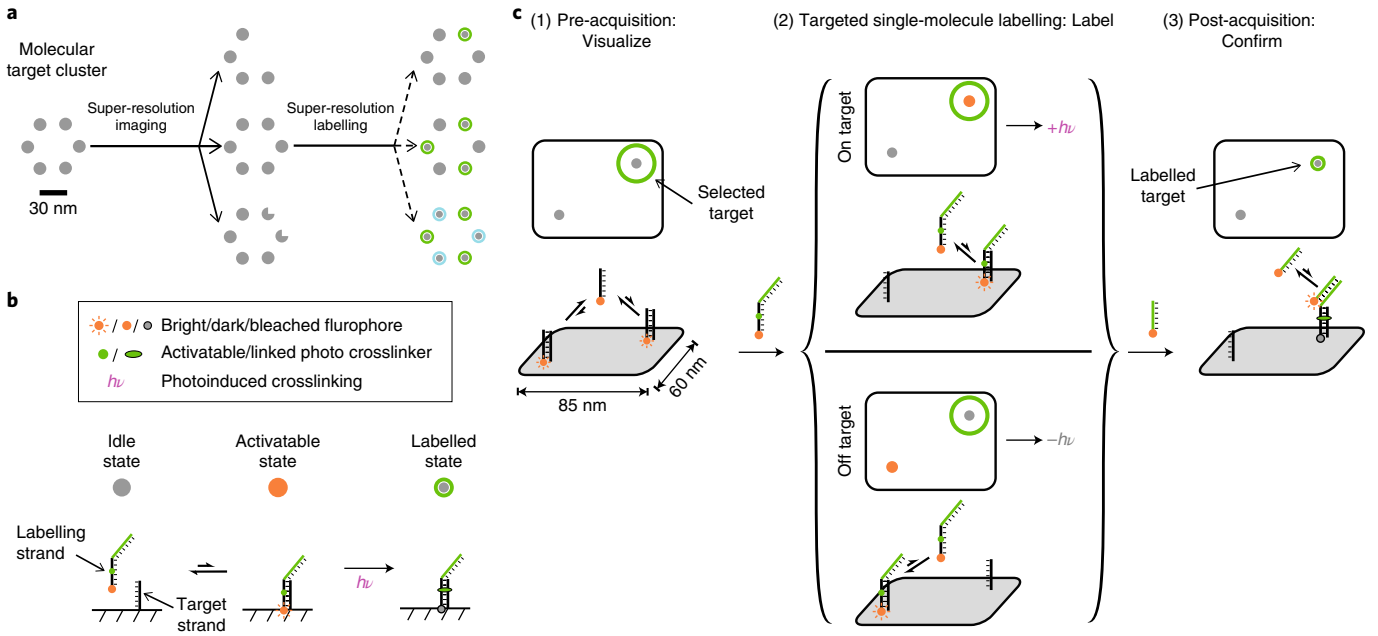


Fig. 1 | Principle of super-resolution single-molecule labelling. a, Schematic illustration of targeted single-molecule labelling upon visualization. Super-resolution imaging allows the visualization and selection of the desired targets of interest among heterogeneous molecular complexes. Subsequent targeted single-molecule labelling allows the precise delivery of molecular cargos or labels to molecular targets in various custom-defined patterns. Grey dots represent individual target molecules (notches represent defects), and the green and cyan halos represent successful molecular labelling (of two kinds). **b**, Strategy to implement single-molecule labelling with DNA-PAINT combined with a photoinducible crosslinker. The crosslinker-bearing, dual-purpose imaging and labelling strand transiently hybridizes to the target strand (between the idle and activatable states). Exposure to the activating light pulse at the activatable state induces the covalent attachment of the molecular label to the target (labelled state). The fluorophore is photobleached in the labelled state, after prolonged illumination. **c**, The experimental workflow for single-molecule labelling with Action-PAINT consists of three steps: (1) to visualize, a super-resolution DNA-PAINT image is captured and candidate target site locations are determined, based on which the experimenter selects the desired labelling target(s); (2) to label, another super-resolution image stack is captured with the labelling strand, accompanied by real-time image processing and automatic crosslinking activation on detection of on-target blinking and (3) to confirm, a final DNA-PAINT image is captured to assay the labelling outcome.

specificity). Thus, we have implemented an effective method for super-resolution labelling upon visualization.

Results

Strategy and workflow for super-resolution labelling with Action-PAINT. We implemented our strategy for super-resolution labelling upon visualization based on our previously developed DNA-PAINT super-resolution microscopy method[12,19] (Supplementary Methods 2.4 gives more details). In brief, the DNA-PAINT method exploits transient binding between short, fluorescently labelled DNA oligonucleotides (the 'imager' strands, in solution) and their complementary strands (the 'docking' strands, labelled on the molecular targets) to produce apparent blinkings when placed under z-confined illumination. With this method, we successfully demonstrated multiplexed three-dimensional (3D) cellular imaging[28], quantitative super-resolution imaging[29] and discrete molecular imaging of molecular features down to ~5 nm in size[19]. Our strategy for Action-PAINT then introduces a fast, photoinduced crosslinking reaction that will be activated at the precise moment (the 'activatable state') when a label-bearing imager strand transiently hybridizes to a selected docking strand of interest, and thereby delivers the molecular label to the desired target site (Fig. 1b).

The experimental workflow for Action-PAINT consists of three steps, and is illustrated as in Fig. 1c (Supplementary Methods 2.5 gives more details). First, to visualize, a pre-acquisition super-resolution image of the target molecular structures is taken with a regular non-crosslinking DNA-PAINT imaging strand that is complementary to the docking strands on the candidate labelling targets. Based on the pre-acquisition image, one or more subdiffraction-sized regions-of-interest (ROIs) around the desired labelling target site(s) are manually selected. Then, to label, a second super-resolution image stack is recorded with a CNVK-bearing dual-purpose imaging and crosslinking strand that also carries a reporter sequence as the molecular label (the 'labelling strand'). This imaging and labelling session is accompanied by a real-time subdiffraction localization, drift correction, image analysis and laser activation control procedure. In particular, a brief pulse of 405 nm illumination is triggered when and only when a labelling strand is detected to be hybridized within the desired target ROIs. The length of the real-time image stack is not preset, and is instead determined by the activation control software based on real-time analysis of the labelling progress and blinking kinetics. Finally, to 'confirm', a post-acquisition image is acquired to assay the labelling correctness and efficiency, with a third imaging strand that is complementary to the delivered reporter sequence. To assist with drift correction, DNA nanostructure drift markers are added alongside the sample, and corresponding imaging strands are supplemented to the imaging buffer for all three imaging steps.

Two technical capabilities are required for the successful implementation of the above strategy. First, a fast and efficient crosslinking agent is needed that can be optically induced to form a covalent crosslink during the transient oligonucleotide hybridization. The CNVK base modification was previously reported[26] to provide a fast crosslinking rate under near-ultraviolet illumination and is compatible for incorporation into oligonucleotides, and thus makes a promising candidate. Second, a real-time image analysis and crosslinking activation control software is needed to reconstruct the super-resolution image and control the prompt activation of

crosslinking illumination on detection of on-target binding. Our previously developed high-accuracy single-molecule localization and drift-correction methods provide a good starting point[19], and can be adapted for real-time analysis.

CNVK crosslinking test and imager design. To assay the crosslinking efficiency of CNVK-modified oligonucleotides on single molecules, we first designed and synthesized cy3b-conjugated CNVK labelling strands (Supplementary Fig. 1; Supplementary Methods 2.3 gives more details). Each CNVK labelling strand serves a dual purpose for both real-time super-resolution imaging and photoinduced crosslinking, and comprises two parts: (1) a DNA-PAINT imaging sequence (that is complementary to the docking sequence on the candidate labelling targets), which contains a CNVK base modification, and (2) an orthogonal DNA-PAINT docking sequence, used as the reporter sequence to assay successful crosslinking. We designed and optimized the CNVK-containing sequence to have an average binding on time of ~1.0 s to be compatible with the crosslinking time constant and imaging frame rate, and thereby maximize the overall crosslinking efficiency (Supplementary Fig. 2; Supplementary Methods 2.3 gives more details).

After confirming the ultraviolet-induced CNVK crosslinking efficiency in bulk with a handheld 365 nm light source and a denaturing gel-shift assay (~50% for a 1 s illumination at 2.5 W cm^{-2} intensity) (Supplementary Fig. 1; Supplementary Methods 2.3 gives more details), we performed a crosslinking efficiency test at the single-molecule level, under typical super-resolution microscopy settings and with 405 nm laser line illumination (~0.5 kW cm^{-2}) (Supplementary Methods 2.3 and 2.4 give more details). We utilized a DNA nanostructure test platform with 12 imaging sites arranged in a rectangular grid pattern, spaced 20 nm point-to-point (the '20 nm grid')[19,30], on which we designed a test pattern with 4 corners as reference markers, and 8 internal sites as candidate labelling targets (Fig. 2a and Supplementary Fig. 3; Supplementary Methods 2.1 gives more details). We then saturated the 20 nm grid samples with CNVK labelling strands, and exposed the sample to a 405 nm laser illumination under a total internal reflection (TIR) configuration. After thoroughly washing the DNA grids of excess crosslinking strands, a post-illumination DNA-PAINT super-resolution image was taken, with an imager strand that is complementary to both the reference corner markers and the reporter sequence on the labelling strand. We then counted the number of labelled targets and calculated a single-molecule crosslinking efficiency of ~45% after a 1 s pulse, which saturates at around ~75% after 15 non-consecutive pulses (1 s each) (Fig. 2b and Supplementary Fig. 4; Supplementary Methods 2.3 gives more details), probably due to combined effects from the self-assembly defects in the DNA nanostructure and an undesired photoinduced crosslinking reversal[27]. We note that this result only reflects the obtainable crosslinking efficiency after a single (transient) oligonucleotide binding event, whereas a potentially higher labelling efficiency could be achieved during a real-time imaging and labelling session after multiple target-binding events and laser crosslinking attempts (for example, an estimated efficiency >90% after up to four binding events, assuming a 1 s average binding on time).

Software design and crosslinking activation control. Next, we developed a software package for real-time super-resolution image analysis and crosslinking activation control (Supplementary Fig. 5; Supplementary Notes 3.1 and Supplementary Methods 2.6 give more details). We adapted our previous off-line, high-precision single-molecule localization and drift correction algorithm for on-line processing. With a moderate single-molecule point spread function fitting precision (~3 nm by the distance between adjacent-frame localizations (DAFL)[19] and <2 nm by single-molecule fitting uncertainty[31]), a ~350 ms frame time was achieved for the complete cycle of data acquisition → super-resolution analysis → laser activation control. The resulting run-time delay for laser activation (~350 ms) was significantly less than the observed blinking on time and crosslinking time constant (Supplementary Fig. 2). A real-time drift correction was achieved by comparing all the super-resolved localizations with DNA grid positions predetermined from the pre-acquisition image (Supplementary Fig. 5; Supplementary Methods 2.6 gives more details). A typical frame-to-frame correction of ~1 nm (root mean square) was observed and corrected. We benchmarked our real-time imaging quality on the 20 nm grid and estimated a residual drift of ~5 nm (root mean square) and a 12–15 nm imaging resolution (Supplementary Fig. 6; Supplementary Notes 3.1.2 and Supplementary Methods 2.6 give more details).

To maximize the selective crosslinking efficiency, the crosslinking laser needs to be stringently controlled, as any off-target illumination or overillumination may result in incorrect or unsuccessful crosslinking. After many rounds of trials and errors, we decided to implement the following laser control scheme to optimize the targeted crosslinking performance (Supplementary Fig. 7; Supplementary Notes 3.1.3 gives more details). First, to make sure that only the desired targets are being labelled, we hand-selected small target regions (circular areas of 20–40 nm diameter, depending on the intertarget separation), centred around both desired ('include-ROI') and undesired ('exclude-ROI') candidate target sites. We only turned on the 405 nm laser when a single-molecule blinking event was detected within one of the include-ROIs, but not in the exclude-ROIs (Fig. 2d). To further prevent the incorrect crosslinking caused by occasional mislocalized blinkings and undesired double-blinking events, we monitored each blinking event (that is, a series of localizations from the same imager strand, imaged in consecutive frames) and excluded any blinking that either originated from or visited one of the exclude-ROIs. Second, we noticed that, although a short blinking event (and a short 405 nm laser pulse) typically results in a low crosslinking efficiency, a prolonged illumination could potentially reverse or damage a previously successful crosslink (Supplementary Notes 3.2 gives more details). Therefore, to maximize the crosslinking success rate, we set a maximum threshold of three seconds of ultraviolet illumination per any single blinking event. Third, each target was considered successfully crosslinked if two criteria were met: (1) the target received at least one frame of 405 nm illumination, (2) no further blinking was observed within the include-ROIs for a set monitor time window of 5–10 minutes. To avoid any unnecessary extra ultraviolet illumination, as well as to maximize the workflow efficiency, the imaging session was automatically terminated by the control software (and reported as successful) as soon as all the target sites passed these criteria; or the session was stopped after a set time out, and reported as unsuccessful.

Super-resolution labelling with 70 nm selectivity. We went on to test our entire Action-PAINT workflow by combining the CNVK-mediated crosslinking with our real-time imaging and labelling control software. We designed a test platform based on the 20 nm grid by positioning two candidate target sites separated by ~70 nm, each surrounded by two reference markers to help identify their positions (Fig. 2c and Supplementary Fig. 3). We note that the two candidate target sites are of identical sequence, and cannot be distinguished from each other by the imager strand, and therefore we expect the binding events to occur at both sites with equal frequency.

Figure 2c,d illustrates a representative successful labelling experiment. Super-resolution images of pre-acquisition real-time labelling and of post-acquisition are shown in Fig. 2c. Analysis of the real-time blinking trace showed only one blinking event on the desired target, which triggered a pulse of 1.0 s (three frames) of 405 nm laser illumination, and resulted in a successful crosslinking

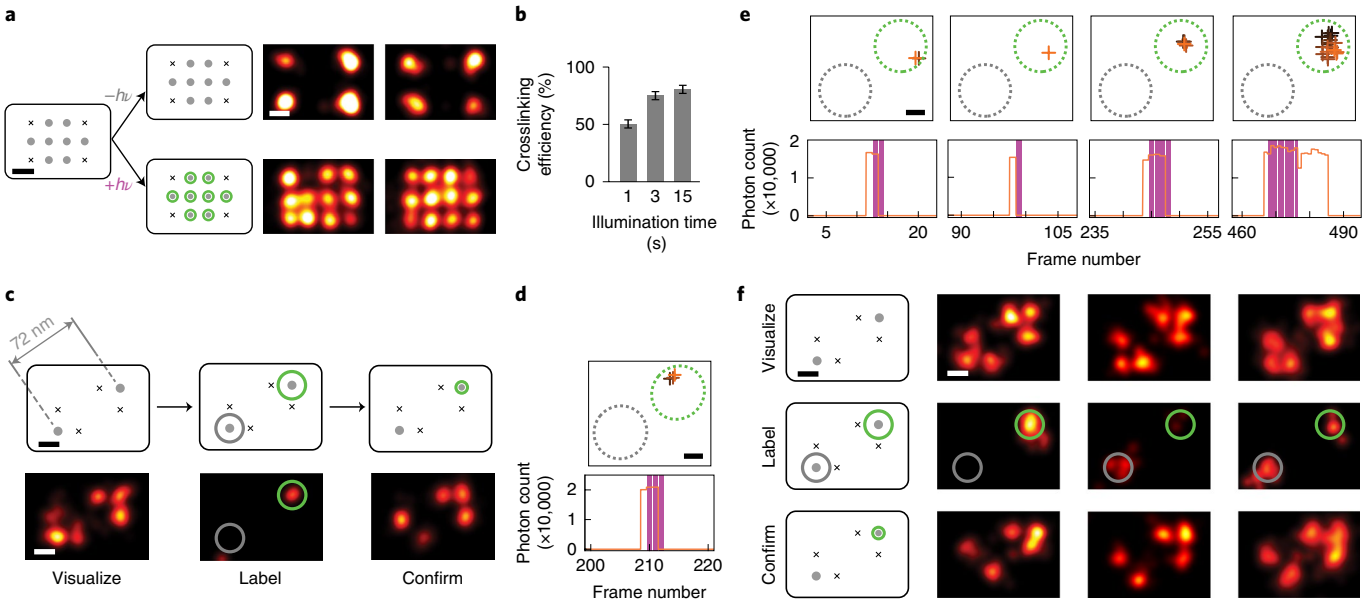


Fig. 2 | Crosslinking efficiency test and targeted single-molecule labelling. a, Test of the CNVK labelling strand crosslinking efficiency on single molecules. Left, DNA nanostructure design with four corner markers and eight central crosslinking targets, spaced 20 nm point-to-point, before and after crosslinking. Right, DNA-PAINT images after crosslinking show the negative control (top) and with a 405 nm laser illumination (bottom). **b**, Crosslinking efficiency comparison for different illumination times. The error bars represent Poisson counting uncertainty (total number of grids counted were 103, 60 and 82, respectively, each with 8 binding sites; the number of labelled targets were 419, 349 and 510, respectively). **c**, Schematics and representative images at different stages of the targeted single-molecule labelling experiment. Top row, schematics of the DNA test structure design with two candidate targets, spaced 72 nm apart; bottom row, super-resolution images. Within the bottom row, the left panel shows a pre-acquisition image of the candidate target sites together with markers, the middle panel shows a real-time labelling session image of the CNVK labelling strand transient blinking events and the right panel shows a post-acquisition image of the labelled targets together with markers. **d**,**e**, Examples of real-time blinking and laser activation traces, which comprise a single blinking event and laser pulse for the sample in **c** (**d**) and a series of four events for the sample in the left column of **f** (**e**). For each detected blinking event, *xy* traces (top) and time traces (bottom) are shown. **f**, Representative examples of successful labelling experiments. Top row, pre-acquisition images; middle row, real-time labelling session images; bottom row, post-acquisition images. In **a**, **c** and **f**, the grey dots without and with a green halo indicate the idle and labelled targets, respectively, the black crosses indicate fixed position markers; large green and grey circles overlaid on the schematics and super-resolution images indicate the desired and undesired target sites, respectively. In **d** and **e**, the *xy* traces are colour coded by time (from black to orange) and overlaid with included (green dotted circles) and excluded (grey dotted circles) ROIs; time traces show the detected photon count per single-molecule localization (orange), overlaid with crosslinking laser illumination events (magenta). Supplementary Note 3.4 discusses the statistics and reproducibility. Scale bars, 20 nm.

onto the target (Fig. 2d). However, not all the labelling attempts were as efficient, and large variations in the total number of laser pulses (or cumulative illumination dosage) were observed from molecule to molecule (Supplementary Fig. 8). Figure 2e shows another representative real-time blinking trace that comprised four consecutive blinking events and four laser pulses (from the sample in Fig. 2f, first column). The first three transient blinking events each triggered a short pulse of 405 nm laser illumination, but did not produce a successful crosslink, as evidenced by the revisitation of the docking site by another crosslinking strand. A fourth, stable blinking event then triggered a long pulse of laser illumination (three seconds, cut by the laser activation threshold) and resulted in successful crosslinking. The prolonged blinking event after the termination of laser activation also suggests a permanent fixation by crosslinking. However, this effect was not always observed and could not be used as a reliable criterion for success (Supplementary Fig. 8). Also, blinking events on the undesired target site did not trigger 405 nm laser activation and no crosslinking took place.

We could only perform targeted labelling experiments on a single DNA grid in an entire field of view, due to a lack of spatial control of laser illumination in our current implementation (note that this current limitation could be overcome by the implementation of a highly parallel labelling approach using a micromirror array). Out of a series of 33 single-molecule labelling trials attempted (Fig. 2f; Supplementary Figs. 8 and 9 give more representative examples of both successful and unsuccessful single-target labelling experiments), 22 were assayed for labelling efficiencies (with post-acquisition), whereas the other 11 were aborted half-way during the real-time imaging session due to early failing signals (such as a misbehaving target site, or occasionally, a damaged DNA nanostructure). We estimated an on-target labelling efficiency of 59% (13 out of 22), and 11 of these trials resulted in correct on-target labelling with no off-target label, which gives a 33% overall success rate and achieves a moderate 3× increase in success rate compared with a random-labelling attempt (expected success rate 10%, assuming a stochastic labelling rate of 11%, as measured from the candidate targets on non-monitored grids in the same experiment). Possible causes for these failed attempts could include the existence of a fraction of dark fluorophores, background crosslinking by the imaging (561 nm) laser or potential 405 illumination-induced damage to the DNA nanostructure (Supplementary Notes 3.2 gives more details). These results demonstrated the ability for single-molecule discrimination and targeted labelling with subdiffraction-limit separation (70 nm, ~1/3× diffraction-limited resolution).

Multiple-point nanoscale patterning with 30 nm selectivity. Next, we sought to demonstrate nanoscale labelling for a more complex multipoint target, and with a closer spatial separation. Such an

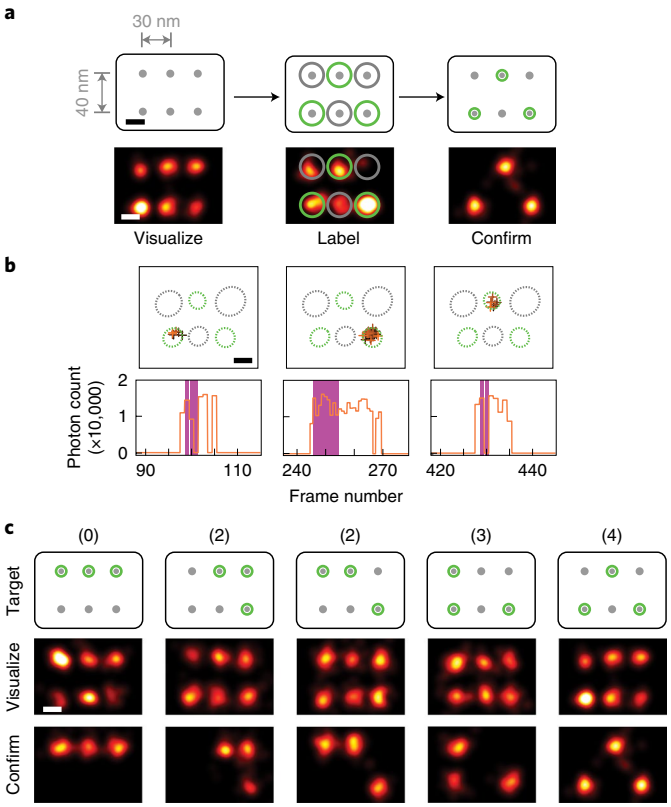


Fig. 3 | Multipoint super-resolution patterning. a, Schematics and representative images at different stages of a targeted three-point single-molecule labelling experiment. Top row, schematics of the DNA test structure design with six candidate targets, spaced 30–40 nm apart; bottom row, super-resolution images. Within the bottom row, the left panel shows a pre-acquisition image of the candidate target sites, the middle panel shows a real-time labelling session image of the CNVK labelling strand transient blinking events and the right panel shows post-acquisition image of labelled targets. **b**, Example of real-time blinking and laser activation traces, which comprises three blinking events on different targets and three laser pulses for the sample in **a**. For each detected blinking event, *xy* traces (top) and time traces (bottom) are shown. **c**, Representative examples of successful three-point patterning experiments for each visually distinct pattern. Top row, schematics of different 6-choose-3 labelling patterns, arranged by increasing difficulty (number of 30 nm spaced pairs necessary to be correctly distinguished for successful patterning); top and middle rows, pre-acquisition images; bottom row, post-acquisition images. The fifth column shows the same experiment as in **a**. In **a** and **c**, the grey dots without and with green halos indicate idle and labelled targets, large green and grey circles overlaid on the schematics and super-resolution images indicate the desired and undesired target sites, respectively. In **b**, the *xy* traces are colour coded by time (from black to orange) and overlaid with include- (green dotted circles) and exclude- (grey dotted circles) ROIs; time traces show the detected photon count per single-molecule localization (orange), overlaid with crosslinking laser illumination events (magenta). Supplementary Note 3.4 discusses the statistics and reproducibility. Scale bars, 20 nm.

effort would require an even more stringent control of the crosslinking laser to avoid any potential off-target crosslinking. Therefore, we further modified the laser control software. First, to ensure a high detection specificity and localization precision, only single-molecule blinkings with a sufficiently long binding on time (at least two frames) and a sufficiently high photon count were considered as candidates for crosslinking. Second, owing to the asynchronous nature of labelling multiple target sites and the potential of photoinduced crosslinking reversal, we extended the no-blinking monitor time limit for individual targets. For those targets that had initially passed the success criteria, but later started to blink again, probably due to crosslinking reversal[27], the monitor and crosslinking workflow was restarted until the criteria were passed for all the targets (Supplementary Fig. 7; Supplementary Notes 3.1.3 gives more details). We also adopted a CNVK purification procedure that was reported to remove a secondary, non-crosslinking species of CNVK[27] (Supplementary Fig. 1; Supplementary Methods 2.3 gives more details).

For this test, we further designed a six-point candidate target pattern with a 30–40 nm point-to-point spacing (Fig. 3a). For each labelling experiment, we first confirmed the presence of all six docking sites during the pre-acquisition, then picked an arbitrary three-point pattern (Fig. 3a) and manually selected the include-ROIs as well as exclude-ROIs accordingly. The real-time imaging and labelling session was then conducted under automatic software control with modified laser activation criteria, as described above.

Figure 3a,b shows a successful three-point patterning experiment. Real-time blinking trace shows three on-target blinking events detected in total; each triggered a pulse of 405 nm laser illumination (~0.6–3 s in length) and resulted in successful crosslinking. Again, not all the attempts were as efficient, and typically a few attempts per target were required for successful crosslinking (Supplementary Fig. 10). Blinking events within the exclude regions (Fig. 3a, middle, grey circles), however, were correctly detected and avoided for off-target crosslinking.

We demonstrated multipoint super-resolution labelling by choosing all five visually distinct three-point patterns on the six-point canvas in Fig. 3c, and achieved successful single-molecule patterning for all cases, which included pre-acquisition and post-acquisition images for each experiment (Fig. 3d; Supplementary Figs. 10 and 11 give more representative examples of both successful and unsuccessful three-point labelling experiments). We performed a total of 84 trials of three-point patterns, out of which 62 were assayed for labelling efficiencies (with post-acquisition) and the other 22 were aborted half-way during the real-time imaging session due to early failing signals (similar to the two-point experiment above). Of the 62 assayed trials, we achieved an overall per-target labelling efficiency of 65%, and a modestly low off-target labelling rate of 15% (Supplementary Notes 3.2.1 gives more details). As a result, 43 of the 62 attempts (69%) were successfully labelled with at least two correct sites, and 61 (98%) had at least one target correctly labelled. Overall, 10 out of 84 trials (12%) produced complete labelling (that is 3 on-target labels and no off-target label). This reflects not only the complexity of the 6-choose-3 pattern, but also a potential crosslinking reversal caused by a prolonged exposure to 405 nm illumination for already crosslinked strands (Supplementary Notes 3.2.2 gives more details). However, compared to a random labelling attempt with the same pattern complexity, we still achieved an 18× increase in the success rate (12% versus 0.66%), assuming a stochastic labelling rate of 25% (as measured from candidate targets on non-monitored grids in the same experiment). We also note that, in future applications, a high labelling and molecular delivery efficiency could be achieved with tandem labelling, for example, up to 69% with twofold and 98% with threefold tandem labelling.

In situ super-resolution labelling on microtubules. Next, we sought to demonstrate the compatibility of Action-PAINT labelling with in situ super-resolution imaging in fixed cultured cells (Fig. 4). To present CNVK crosslinking strands on immunostained targets (microtubules), we prepared a secondary antibody that is directly conjugated to the labelling target strand. After immunostaining, the Action-PAINT workflow was conducted in a similar way as above (Fig. 4a), but with two important differences. First,

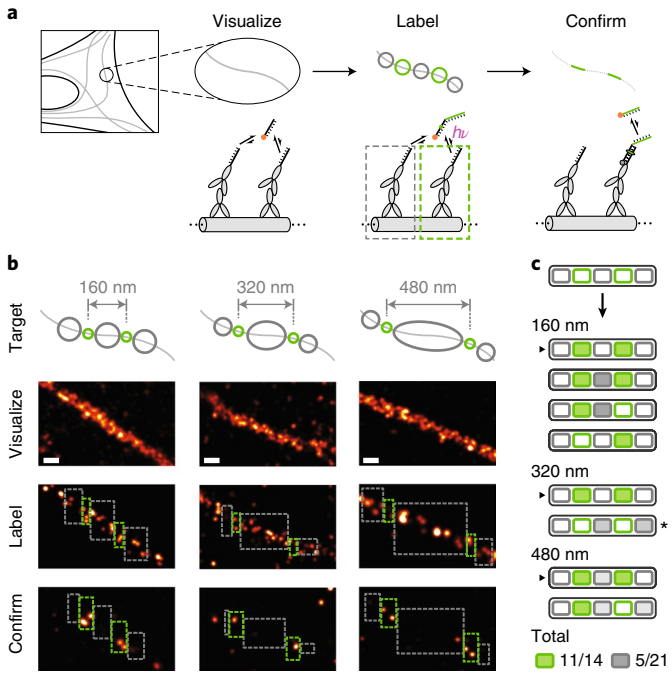


Fig. 4 | In situ super-resolution labelling on microtubules. a, Schematics and workflow of super-resolution labelling on immunostained and DNA-labelled microtubule samples in fixed BSC-1 cells. **b**, Examples of successful two-target patterning on microtubules for different intertarget spacings. Top row, schematics of the desired labelling patterns; second row, pre-acquisition images; third row, real-time labelling session images; bottom row, post-acquisition images. **c**, Schematic list of the outcome of eight experimental trials. Successfully labelled targets are shaded green, and undesired labels in exclude areas are shaded different levels of grey to reflect the difference in the exclude area. Arrows indicate the experiments shown in **b**. *Experiment excluded from the statistics, due to a likely sample movement based on a visual observation of an apparent change in the microtubule morphology between pre- and post-acquisition sessions. In all panels, the green and grey circles in the schematics indicate the desired and undesired targets, respectively; the green and grey dashed rectangles indicate experimental include- and exclude-ROIs, respectively. ROIs in bottom rows (post-acquisition images) are adjusted by a 20 nm edge buffer, according to the overall localization and labelling precision. Supplementary Fig. 13 gives more examples of the microtubule labelling experiments and Supplementary Fig. 14 gives more details on the labelling efficiency and specificity. Supplementary Methods and Supplementary Notes 3.3 give more details on the crosslinking efficiency and specificity calculation, and on edge-buffered ROIs, and Supplementary Notes 3.4 discusses the statistics and reproducibility. Scale bars, 100 nm.

instead of placing the candidate target sites individually at regularly spaced grid patterns, we placed them continuously along the microtubules, which results in large 'patches' of labelling target sites. Consequently, it was not possible to distinguish among them and select a target ROI that contained a single target site; instead, each target ROI likely contained more than one labelling target. Second, owing to the unknown multiplicity of target sites, it was difficult to assay the degree of crosslinking during the real-time labelling session using the same blinking kinetics analysis as before. Therefore, we either conducted fixed-length real-time labelling sessions or employed a different set of stopping criteria based on the total dose of crosslinking illumination received on the target.

To assay our 'batch' crosslinking efficiency and specificity on immunostained microtubules, we selected two relatively large include-ROIs (~160 nm, each containing a number of candidate labelling sites) flanked by three similar-sized exclude-ROIs and conducted a real-time labelling session with a few different lengths (Supplementary Fig. 12). In each case, we observed multiple successful labels within the include-ROIs. However, we also observed a significant fluctuation in the overall labelling efficiency, as well as several off-target labels in exclude-ROIs, probably caused by background crosslinking from the 561 nm imaging laser. We reasoned that a smaller include-ROI together with a shorter labelling session length would reduce the total dose of illumination from both the crosslinking and imaging lasers, and thus allow a more uniform and specific labelling. Indeed, with a reduced target ROI size (~80 nm) and a shorter labelling session, we achieved a 90% on-target labelling efficiency (9 out of 10) with a moderate 33% off-target labelling (5 out of 15) (Supplementary Fig. 12).

Next, we sought to demonstrate the controlled super-resolution targeting ability of Action-PAINT on immunostained microtubules by patterning three pairs of labels with different, diffraction-unlimited spacing (from 160 to 480 nm, Fig. 4b and Supplementary Fig. 13). For these experiments, we further reduced the target ROI size to ~40 nm (each including a small number of target sites only) and employed the following stopping criteria: (1) each target ROI should receive at least three separate crosslinking illuminations and (2), ideally, at least one of the illuminations should last for two imaging frames or longer. To limit the extent of background crosslinking induced by the imaging laser, we also set a limit on the total number of frames for the real-time labelling session (Supplementary Notes 3.1.4 give more details). Out of 7 valid labelling trials, we achieved an overall 78% on-target labelling efficiency (11 out of 14), and maintained a moderate 24% off-target labelling (5 out of 21), even with a much larger exclude-ROI area (Fig. 4c). We further quantified our labelling efficiency and specificity on a per-target basis by comparing the number of recorded DNA-PAINT localizations in each include- or exclude-ROI before and after Action-PAINT labelling (that is, from the pre- and post-acquisition images, the ROI areas were adjusted with edge buffers (Supplementary Methods and Supplementary Notes 3.3 give more details). On average, we achieved an ~4.2× (median) per-target enrichment (on target versus off target) in labelling efficiency (Supplementary Fig. 14), similar to our earlier observation (~4.3×) on synthetic DNA nanostructures.

Discussion

Here we demonstrated super-resolution labelling and patterning with Action-PAINT, which enables targeted single-molecule labelling upon visualization—that is, successive super-resolution imaging followed by targeted labelling—at the single-molecule scale. Such a method allows biological researchers to not only 'see the previously invisible', but also 'touch the previously inaccessible', and could open up a broad range of new biological investigations. In our implementation, we combined real-time DNA-PAINT super-resolution microscopy and fast, photoinducible crosslinking chemistry (CNVK) to achieve this goal. We demonstrated a successful targeted single-molecule labelling with a 30–70 nm spatial selectivity and a high (59–65%) on-target labelling efficiency on a synthetic DNA nanostructure breadboard. For single-target labelling, we achieved an overall 33% success rate (3× higher compared to random labelling); for complex multipoint patterning (6-choose-3 targets), we achieved a high success rate (69%) for at least two on-target labels and for perfect labelling (that is, 3 on-target labels, no off-target label) an overall 12% success rate (18× higher compared to random labelling). We also demonstrated the compatibility of our Action-PAINT method with in situ super-resolution imaging and performed successful targeted labelling of cellular targets with a 40 nm label size and variable, diffraction-unlimited spacings. On microtubule samples fixed and immunostained with oligoconjugated antibodies that present the CNVK-containing crosslinking targets, we achieved an overall 78% on-target labelling efficiency,

with a moderate 24% off-target labelling. We further quantified a normalized on-/off-target labelling specificity of ~4.2× (median) for in situ labelling on microtubules, comparable to our earlier observation (~4.3×) on synthetic DNA nanostructures. Our method can be naturally adapted for multiplexed super-resolution labelling on multiple molecular targets by exploiting programmable orthogonal binding sequences[28], and for 3D imaging and targeted single-molecule labelling with the application of point spread function engineering approaches (such as astigmatism[32] or a double-helix point spread function[33]).

Compared with other nanoscale patterning strategies, such as electron-beam lithography or atomic force microscopy, Action-PAINT is a less disruptive, light-based labelling technique that uses only standard wavelengths (405 nm and 561 nm) found on common commercially available microscopes. Although light-based subdiffraction patterning has been previously demonstrated for potential high-capacity optical storage applications (by switching off reversibly photoswitchable green fluorescent protein molecules with the RESOLFT method[34]), such a 'super-resolution writing' approach does not label or modify the targets with a physical, molecular handle. In contrast, Action-PAINT delivers a physical, addressable handle to the target of interest, which enables subsequent analysis and manipulation of the labelled targets—critical for downstream perturbation or physical manipulation to the biological system, for example, by target-specific small-molecule inhibitor delivery or handle attachment— which thus makes Action-PAINT a valuable tool for the precision interrogation of biological systems.

Further development of this technology probably needs to address two current technical limitations. One is that, due to the lack of spatial control of the crosslinking laser (currently uniformly illuminated across the entire field of view), selective single-molecule labelling could only be achieved within a small fraction of the field (up to a few diffraction-limited areas). To overcome this limitation, and thus allow efficient, highly parallel custom labelling across multiple desired ROIs, an automated digital micromirror device could be implemented to independently control the delivery of the activation laser at every diffraction-limited area across the field of view, and thus allow up to a million single-molecule monitoring and labelling sessions in parallel. Another current limitation is the crosslinking efficiency, which ultimately constrains the overall labelling success rate and achievable patterning complexity. Possible options for improvement include using double CNVK-modified strands or a more efficient photoinducible crosslinking chemistry. Supplementary Fig. 15 shows in silico simulation that compares the effect of different experimental conditions, which include the number of include- and exclude-ROIs, characteristic binding on time and off time, and total imaging session length on the overall Action-PAINT success rate.

We envision that user-defined, single-molecule labelling with Action-PAINT will provide a valuable tool for the precise probing of biomolecular targets. Owing to the highly heterogeneous and context-dependent nature of many biomolecular systems (such as the cellular cytoskeletal network, membrane protein clusters, cytosolic mRNAs distribution and chromosome 3D architecture), a meaningful perturbation and manipulation can only be performed based on knowledge of the particular biological system in question, which cannot be obtained a priori. Action-PAINT could provide the unique conceptual advantage that would allow targeting and perturbation decisions to be based on real-time imaging data and informed by context-relevant features, such as neighbouring cytoskeletal architecture, protein distribution and interaction patterns, or by nucleic acid sequence-specific features, such as topologically associated domains within the chromosome 3D structure, and be performed at a super-resolution, single-molecule level. We outline below two future directions of targeted biological perturbation and manipulation that could be potentially enabled by Action-PAINT.

One would involve quantitative studies of the effects of cell membrane receptor and ion channel activation at the super-resolution and single-molecule level, which have thus far been limited, due to a lack of manipulation tools that allow super-resolution activation and inhibition on the single-molecule level and stoichiometric delivery of small molecule effectors. Such studies are especially important in neurons, for which various studies have implied a functional significance of individual ion channels in affecting neuron generation, action potential stabilization and spike shape, as well as the effects of ion channel clustering on local ion concentration and downstream neurotransmitter signalling[35,36]. Compared with current super-resolution microscopy methods that allow visualization at the nanoscale and optogenetic tools that allow diffraction-limited ion channel perturbation, Action-PAINT-based methods could potentially allow a precise activation and inhibition of individual ion channels (such as with the delivery of a single peptide toxin molecule) within crowded molecular environments. Combined with fast (subsecond) super-resolution imaging and analysis[37], Action-PAINT could potentially be extended to follow single molecules in motion and perform targeted labelling on them (with simultaneous super-resolution imaging), which is suitable for targeting single ion channels during slow or cytoskeleton-confined diffusion[38]. Further, Action-PAINT could potentially allow the study of the cooperative effects between multiple ion channels within the same cluster, and between multiple types of different ion channels.

Another future direction would involve batch studies of proteins and protein complexes selected using imaging-based criteria, including subcellular or suborganelle localization, or cytoskeleton and protein interaction patterns. Action-PAINT could allow imaging-based identification followed by targeted labelling of all the protein targets of interest with a universal handle (for example, biotin or a unique DNA handle). After handle-based extraction and purification, a wide range of downstream analysis and manipulation could be envisioned, including extraction of labelled proteins for analysis by chromatography or single-molecule protein array[39], and potential in situ proteomic analysis with mechanical force spectroscopy. One such example could be to study the different location- and direction-dependent binding partners of kinesin and dynein using a combination of high-throughput Action-PAINT and the emerging single-molecule methods for protein identifications, and thus build a protein–protein interaction map based on subcellular localization information that is currently unachievable. Using uniquely encoded DNA handle sequences, proteins that reside in multiple cellular locations or exhibit multiple interaction patterns could also be precisely encoded and separately extracted for analysis, which potentially enables a novel 'imaging-based proteomics' approach that has not been possible with current biochemical[40] and super-resolution microscopy methods.

Reporting summary. Further information on research design is available in the Nature Research Reporting Summary linked to this article.

Data availability

Datasets generated during the study are available from the corresponding authors upon request.

Code availability

Custom computer programs used during the study are available from the corresponding authors upon request.

Received: 16 April 2018; Accepted: 5 August 2019;
Published online: 16 September 2019

References

1. Sahl, S. J. & Moerner, W. Super-resolution fluorescence imaging with single molecules. *Curr. Opin. Struc. Biol.* **23**, 778–787 (2013).

2. Sydor, A. M., Czymmek, K. J., Puchner, E. M. & Mennella, V. Super-resolution microscopy: from single molecules to supramolecular assemblies. *Trends Cell Biol.* **25**, 730–748 (2015).
3. Eggeling, C., Willig, K. I., Sahl, S. J. & Hell, S. W. Lens-based fluorescence nanoscopy. *Q. Rev. Biophys.* **48**, 178–243 (2015).
4. Sanders, D. P. Advances in patterning materials for 193 nm immersion lithography. *Chem. Rev.* **110**, 321–360 (2010).
5. Cohen, A. E. Optogenetics: turning the microscope on its head. *Biophys. J.* **110**, 997–1003 (2016).
6. Ando, T., Uchihashi, T. & Scheuring, S. Filming biomolecular processes by high-speed atomic force microscopy. *Chem. Rev.* **114**, 3120–3188 (2014).
7. Rust, M. J., Bates, M. & Zhuang, X. Sub-diffraction-limit imaging by stochastic optical reconstruction microscopy (STORM). *Nat. Methods* **3**, 793–795 (2006).
8. Heilemann, M. et al. Subdiffraction-resolution fluorescence imaging with conventional fluorescent probes. *Angew. Chem. Int. Ed.* **47**, 6172–6176 (2008).
9. Betzig, E. et al. Imaging intracellular fluorescent proteins at nanometer resolution. *Science* **313**, 1642–1645 (2006).
10. Hess, S. T., Girirajan, T. & Mason, M. D. Ultra-high resolution imaging by fluorescence photoactivation localization microscopy. *Biophys. J.* **91**, 4258–4272 (2006).
11. Sharonov, A. & Hochstrasser, R. M. Wide-field subdiffraction imaging by accumulated binding of diffusing probes. *Proc. Natl Acad. Sci. USA* **103**, 18911–18916 (2006).
12. Jungmann, R. et al. Single-molecule kinetics and super-resolution microscopy by fluorescence imaging of transient binding on DNA origami. *Nano Lett* **10**, 4756–4761 (2010).
13. Löschberger, A. et al. Super-resolution imaging visualizes the eightfold symmetry of gp210 proteins around the nuclear pore complex and resolves the central channel with nanometer resolution. *J. Cell Sci.* **125**, 570–575 (2012).
14. Szymborska, A. et al. Nuclear pore scaffold structure analyzed by super-resolution microscopy and particle averaging. *Science* **341**, 655–658 (2013).
15. Pertsinidis, A. et al. Ultrahigh-resolution imaging reveals formation of neuronal SNARE/Munc18 complexes in situ. *Proc. Natl Acad. Sci. USA* **110**, E2812–E2820 (2013).
16. Huang, F. et al. Ultra-high resolution 3D imaging of whole cells. *Cell* **166**, 1028–1040 (2016).
17. Kaplan, C. et al. Absolute arrangement of subunits in cytoskeletal septin filaments in cells measured by fluorescence microscopy. *Nano Lett.* **15**, 3859–3864 (2015).
18. Mikhaylova, M. et al. Resolving bundled microtubules using anti-tubulin nanobodies. *Nat. Commun.* **6**, 7933 (2015).
19. Dai, M., Jungmann, R. & Yin, P. Optical imaging of individual biomolecules in densely packed clusters. *Nat. Nanotechnol.* **11**, 798–807 (2016).
20. Raab, M., Schmied, J. J., Jusuk, I., Forthmann, C. & Tinnefeld, P. Fluorescence microscopy with 6 nm resolution on DNA origami. *Chemphyschem* **15**, 2431–2435 (2014).
21. Rittweger, E., Han, K., Irvine, S. E., Eggeling, C. & Hell, S. W. STED microscopy reveals crystal colour centres with nanometric resolution. *Nat. Photon.* **3**, 144–147 (2009).
22. Giannone, G. et al. Dynamic superresolution imaging of endogenous proteins on living cells at ultra-high density. *Biophys. J.* **99**, 1303–1310 (2010).
23. Schoen, I., Ries, J., Klotzsch, E., Ewers, H. & Vogel, V. Binding-activated localization microscopy of DNA structures. *Nano Lett.* **11**, 4008–4011 (2011).
24. Kiuchi, T., Higuchi, M., Takamura, A., Maruoka, M. & Watanabe, N. Multitarget super-resolution microscopy with high-density labeling by exchangeable probes. *Nat. Methods* **12**, 743–746 (2015).
25. Barish, R. & Yin, P. Methods and compositions relating to optical super-resolution patterning. US patent 10,041,108 (2018).
26. Yoshimura, Y. & Fujimoto, K. Ultrafast reversible photo-cross-linking reaction: toward in situ DNA manipulation. *Org. Lett.* **10**, 3227–3230 (2008).
27. Vieregg, J. R., Nelson, H. M., Stoltz, B. M. & Pierce, N. A. Selective nucleic acid capture with shielded covalent probes. *J. Am. Chem. Soc.* **135**, 9691–9699 (2013).
28. Jungmann, R. et al. Multiplexed 3D cellular super-resolution imaging with DNA-PAINT and Exchange-PAINT. *Nat. Methods* **11**, 313–318 (2014).
29. Jungmann, R. et al. Quantitative super-resolution imaging with qPAINT. *Nat. Methods* **13**, 439–442 (2016).
30. Rothemund, P. W. Folding DNA to create nanoscale shapes and patterns. *Nature* **440**, 297–302 (2006).
31. Smith, C. S., Joseph, N., Rieger, B. & Lidke, K. A. Fast, single-molecule localization that achieves theoretically minimum uncertainty. *Nat. Methods* **7**, 373–375 (2010).
32. Huang, B., Wang, W., Bates, M. & Zhuang, X. Three-dimensional super-resolution imaging by stochastic optical reconstruction microscopy. *Science* **319**, 810–813 (2008).
33. Pavani et al. Three-dimensional, single-molecule fluorescence imaging beyond the diffraction limit by using a double-helix point spread function. *Proc. Natl Acad. Sci. USA* **106**, 2995–2999 (2009).
34. Grotjohann, T. et al. Diffraction-unlimited all-optical imaging and writing with a photochromic GFP. *Nature* **478**, 204–208 (2011).
35. Dorval, A. D. & White, J. A. Channel noise is essential for perithreshold oscillations in entorhinal stellate neurons. *J. Neurosci.* **25**, 10025–10028 (2005).
36. Cao, Y.-Q. et al. Presynaptic Ca^{2+} channels compete for channel type-preferring slots in altered neurotransmission arising from Ca^{2+} channelopathy. *Neuron* **43**, 387–400 (2004).
37. Huang, F. et al. Video-rate nanoscopy using sCMOS camera-specific single-molecule localization algorithms. *Nat. Methods* **10**, 653–658 (2013).
38. Albrecht, D. et al. Nanoscopic compartmentalization of membrane protein motion at the axon initial segment. *J. Cell Biol.* **215**, 37–46 (2016).
39. Rondelez, Y. et al. Microfabricated arrays of femtoliter chambers allow single molecule enzymology. *Nat. Biotechnol.* **23**, 361–365 (2005).
40. Rhee, H.-W. et al. Proteomic mapping of mitochondria in living cells via spatially restricted enzymatic tagging. *Science* **339**, 1328–1331 (2013).

Acknowledgements

The authors thank R. Barish, H. Soundarajan, S. Agasti, J. Woehrstein and R. Jungmann for preliminary work on aspects of earlier versions of the project and for helpful discussions, and W. Shih, H. Sasaki, B. Beliveau, E. Boyden and J. Paulsson for helpful discussions. This work was supported by a National Institutes of Health (NIH) Director's New Innovator Award (1DP2OD007292), an NIH Transformative Research Award (1R01EB018659), an NIH Pioneer Award (1DP1GM133052), an NIH grant (5R21HD072481), an Office of Naval Research (ONR) Young Investigator Program Award (N000141110914), ONR grants (N000141010827, N000141310593 and N000141812549), a National Science Foundation (NSF) Faculty Early Career Development Award (CCF1054898), an NSF grant (CCF1162459) and the Molecular Robotics Initiative fund at the Wyss Institute for Biologically Engineering Faculty to P.Y. M.D. acknowledges support from a HHMI International Predoctoral Fellowship, Department Fellowship from Systems Biology Department at the Harvard Medical School, and a Technology Development Fellowship from the Wyss Institute at Harvard University. S.K.S. acknowledges support from a Human Frontier Science Program (HFSP) fellowship (LT000048/2016-L).

Author contributions

M.D. and P.Y. conceived and designed the study, N.L. and M.D. designed and performed the experiments and analysed the data, M.D. developed the software, S.K.S. provided advice and assistance with the microtubule sample preparation. P.Y. supervised the study. All the authors wrote and approved the manuscript.

Competing interests

A US patent (US App No. 15/104,570) has been filed that covers the concepts reported in this work (inventors, R. Barish and P.Y.). P.Y. is cofounder of Ultivue Inc. and NuProbe Global.

Additional information

Supplementary information is available for this paper at https://doi.org/10.1038/s41557-019-0325-7.

Correspondence and requests for materials should be addressed to M.D. or P.Y.

Reprints and permissions information is available at www.nature.com/reprints.

Publisher's note Springer Nature remains neutral with regard to jurisdictional claims in published maps and institutional affiliations.

© The Author(s), under exclusive licence to Springer Nature Limited 2019

nature research

Corresponding author(s): Peng Yin, Mingjie Dai

Last updated by author(s): Jul 9, 2019

Reporting Summary

Nature Research wishes to improve the reproducibility of the work that we publish. This form provides structure for consistency and transparency in reporting. For further information on Nature Research policies, see Authors & Referees and the Editorial Policy Checklist.

Statistics

For all statistical analyses, confirm that the following items are present in the figure legend, table legend, main text, or Methods section.

n/a	Confirmed	
☒	☐	The exact sample size (*n*) for each experimental group/condition, given as a discrete number and unit of measurement
☒	☐	A statement on whether measurements were taken from distinct samples or whether the same sample was measured repeatedly
☒	☐	The statistical test(s) used AND whether they are one- or two-sided *Only common tests should be described solely by name; describe more complex techniques in the Methods section.*
☒	☐	A description of all covariates tested
☒	☐	A description of any assumptions or corrections, such as tests of normality and adjustment for multiple comparisons
☐	☒	A full description of the statistical parameters including central tendency (e.g. means) or other basic estimates (e.g. regression coefficient) AND variation (e.g. standard deviation) or associated estimates of uncertainty (e.g. confidence intervals)
☒	☐	For null hypothesis testing, the test statistic (e.g. *F*, *t*, *r*) with confidence intervals, effect sizes, degrees of freedom and *P* value noted *Give P values as exact values whenever suitable.*
☒	☐	For Bayesian analysis, information on the choice of priors and Markov chain Monte Carlo settings
☒	☐	For hierarchical and complex designs, identification of the appropriate level for tests and full reporting of outcomes
☒	☐	Estimates of effect sizes (e.g. Cohen's *d*, Pearson's *r*), indicating how they were calculated

Our web collection on statistics for biologists contains articles on many of the points above.

Software and code

Policy information about availability of computer code

Data collection	Data collection was performed using Nikon Elements software (AR 4.51.01) along with SDK (v4.4.1.728), and custom computer programs (MATLAB 2015a) which will be made available upon request.
Data analysis	Data analysis was performed using custom computer programs (MATLAB 2015a) which will be made available upon request.

For manuscripts utilizing custom algorithms or software that are central to the research but not yet described in published literature, software must be made available to editors/reviewers. We strongly encourage code deposition in a community repository (e.g. GitHub). See the Nature Research guidelines for submitting code & software for further information.

Data

Policy information about availability of data

All manuscripts must include a data availability statement. This statement should provide the following information, where applicable:

- Accession codes, unique identifiers, or web links for publicly available datasets
- A list of figures that have associated raw data
- A description of any restrictions on data availability

Data sets generated during the study will be made available upon request.

Field-specific reporting

Please select the one below that is the best fit for your research. If you are not sure, read the appropriate sections before making your selection.

☒ Life sciences ☐ Behavioural & social sciences ☐ Ecological, evolutionary & environmental sciences

Life sciences study design

All studies must disclose on these points even when the disclosure is negative.

Sample size	We only performed aggregate counting on the results, and did not perform statistical significance analysis between two groups of conditions. Samples sizes for Action-PAINT experiments on DNA origami grids in vitro were not pre-determined, multiple experiments were performed until at least n=10 successes were achieved for both the 2-choose-1 and 6-choose-3 paradigm of experiments. Accordingly, success rate and sample size statistics were calculated for all attempts (both successful or unsuccessful) and compared to expected labeling efficiency of stochastic labeling. Sample sizes for Action-PAINT experiments on microtubules were set to n>=2 for each condition. We found that all microtubule labeling experiments across all conditions showed positive enrichment of labeling in the include region vs exclude region.
Data exclusions	Only one data point was excluded for the microtubule labelling experiment (which was illustrated in Fig. 4c and indicated by *, and raw data for this experiments was shown in Fig. S13), due to likely unintentional sample movement in between labelling and post-acquisition sessions. Since this is a new method, there was no previous established exclusion criteria available.
Replication	All replication attempts and outcomes (number of overall successes, number of successfully and unsuccessfully labelled targets) are reported for each experimental test conditions (Supplementary Notes 3.4). Reasons for unsuccessful labeling attempts are hypothesized and described in the supplemental file (Supplemental Notes 3.2). The experiment to produce the first pattern in Figure 3C (first column) was only performed once for visualization purposes for a specific case where all DNA sites on this grid were 40 nm away from exclusion sites due to DNA origami design constraints. Thus this pattern was not equivalent to the other patterns which had at least two sites 30 nm away from an exclusion site that we tested more robustly for the experiments we provide.
Randomization	We did not perform statistical analysis between groups of different conditions.
Blinding	We did not perform statistical analysis between groups of different conditions.

Reporting for specific materials, systems and methods

We require information from authors about some types of materials, experimental systems and methods used in many studies. Here, indicate whether each material, system or method listed is relevant to your study. If you are not sure if a list item applies to your research, read the appropriate section before selecting a response.

Materials & experimental systems

n/a	Involved in the study
☐	☒ Antibodies
☐	☒ Eukaryotic cell lines
☒	☐ Palaeontology
☒	☐ Animals and other organisms
☒	☐ Human research participants
☒	☐ Clinical data

Methods

n/a	Involved in the study
☒	☐ ChIP-seq
☒	☐ Flow cytometry
☒	☐ MRI-based neuroimaging

Antibodies

Antibodies used	Rat anti-alpha-tubulin YL1/2 (ThermoFisher Invitrogen, MA1-80017, Lot # TJ2652992), used at 1:50 dilution. Donkey anti-Rat IgG (H+L) (Jackson Immuno Research AffiniPure, 712-005-153, Lot Lot # 139472), used at 1:50 dilution after conjugation.
Validation	Rat anti-alpha-tubulin antibody was tested by ThermoFisher for immunofluorescence applications and used in previous publications in fixed human cells. This clone recognizes the alpha subunit of tubulin, specifically binding tyrosylated Tubulin. See website for details: https://www.thermofisher.com/antibody/product/alpha-Tubulin-Antibody-clone-YL1-2-Monoclonal/MA1-80017

Eukaryotic cell lines

Policy information about cell lines

Cell line source(s)	BS-C-1 (monkey, ATCC CCL-26)
Authentication	This cell line has not been authenticated.
Mycoplasma contamination	Cell lines were not tested for mycoplasma contamination but no indication of contamination was observed.

Commonly misidentified lines (See ICLAC register)	No commonly misidentified cell lines were used.